Determination of Heat of Transformation in a Cold-Rolled Martensitic TiNi Alloy

H.C. LIN and S.K. WU

We studied the heat of transformation, ΔH, in martensitic transformations in a cold-rolled equiatomic TiNi alloy with differential scanning calorimetry (DSC), X-ray diffraction (XRD), and microhardness measurements. Results of our experiment indicate that the martensite stabilization and stress-induced parent (SIP) $B2$ phase are introduced when the TiNi martensite is cold rolled at room temperature. The SIP formation seems to be related to the lattice softening phenomenon occurring in the martensite, while the ΔH value of the first reverse martensitic transformation decreases enormously for the cold-rolled equiatomic TiNi alloy. We are proposing possible explanations for these results: (1) the occurrence of SIP, which reduces the transformable martensite volume; (2) the release of accumulated elastic energy induced by the cold rolling; and (3) the recovery of defects induced by cold rolling and release of the heat of recovery. We also found that the retained dislocations can depress the martensitic transformation temperatures and induce the R-phase transformation after the occurrence of the first reverse martensitic transformation.

I. INTRODUCTION

AMONG many shape memory alloys, TiNi alloys are the most popular because they can be deformed in a ductile manner to more than 50 pct strain prior to fracture and show the shape memory effect or pseudoelasticity (PE) over a wide range of strain up to 8 pct.[1] The transformation behavior and mechanical properties in TiNi binary alloys[2–6] and TiNiX ternary alloys[7–10] have been studied extensively. These studies have confirmed that transformation behaviors and mechanical properties can be affected by internal stresses induced by many thermal-mechanical treatments, including thermal cycling,[11,12] aging treatment in Ni-rich alloys,[13–16] and annealing immediately following cold working.[17,18]

Many recent articles have reported deformation behavior and stress effects in TiNi alloys[17,18,20,21] and stated that the stress in these alloys significantly affects the start and finish transformation temperatures and induces the R-phase transformation and that the microstructure with dislocations or precipitates impedes the movement of martensite interfaces and depresses the M_s point. All of these reported studies, however, were conducted on TiNi specimens which had been deformed with subsequent annealing. TiNi specimens that have been deformed but not annealed are seldom studied, although some results have been implied in the reports.[22,23,24] In our previous article,[19] we discussed the effects of cold rolling on the martensitic transformation of equiatomic TiNi alloy primarily through transmission electron microscope (TEM) observation and internal friction measurement. We observed the phenomenon of martensite stabilization in the cold-rolled $Ti_{50}Ni_{50}$ alloy at room temperature. We expected the deformed structures, such as distorted martensite and dislocations/vacancies, to impede the reverse martensitic transformation by imposing a frictional stress on the martensite/martensite and martensite/parent interfaces. This would cause the reverse martensitic transformation temperatures to shift to higher values, since the transformation would require additional driving force to overcome the frictional stress. In this study, we plastic-deformed the equiatomic TiNi alloy by cold rolling at room temperature and then conducted differential scanning calorimetry (DSC), X-ray diffraction (XRD), and microhardness measurements. In the following sections, we systematically describe the transformation heat exhibited in this deformed TiNi alloy and its relation to the degree of cold rolling.

II. EXPERIMENTAL PROCEDURE

We used the conventional tungsten arc melting technique to prepare the equiatomic TiNi alloy. Titanium (purity, 99.7 pct) and nickel (purity, 99.9 pct), totalling about 60 g, were melted and remelted at least six times in an argon atmosphere. Pure titanium buttons were also melted and used as a getter. The mass loss during melting was negligible. The as-melted button was homogenized at 1050 °C for 72 hours and quenched in water, then hot-rolled to a plate of 3-mm thickness. Specimens for cold rolling were carefully cut from the plate with a low-speed diamond saw. These specimens were then annealed at 800 °C for 2 hours and cooled in a vacuum furnace. After annealing, some specimens were cold-rolled at room temperature to a 5, 10, 20, and 40 pct reduction in thickness and then subjected to the DSC, XRD, and microhardness measurements. The temperature increase in the specimens during the cold-rolling process was very slight, even in the 40 pct thickness-reduced specimen.

A Du Pont 9990 thermal analyzer equipped with a quantitative scanning system 910 DSC cell was used to run controlled heating and cooling on samples encapsulated in an aluminum pan. Temperatures ranged from −60 °C to +300 °C with a heating/cooling rate of 10 °C/min. The heat of transformation, ΔH, was automatically calculated from the area under the DSC peak

H.C. LIN, formerly Graduate Student, Institute of Materials Science and Engineering, National Taiwan University, is Assistant Professor, Department of Materials Science, Feng Chia University, Taichung, Taiwan, Republic of China. S.K. WU, Professor, is with the Institute of Materials Science and Engineering, National Taiwan University, Taipei, Taiwan 106, Republic of China.

Manuscript submitted April 20, 1992.

with the equipment software packages. The XRD analysis was carried out at room temperature with the PHILIPS* PW1710 X-ray diffractometer under the conditions of CuKα radiation, 30 kV tube voltage, and 20 mA current. The specimen size for XRD was 20 by 20 mm. Specimens for the hardness testing were mechanically polished and then measured in the Vickers microhardness tester with a 1000-g load at room temperature. For each specimen, the hardness value, Hv, was averaged from at least five test readings.

*PHILIPS is a trademark of Philips Electronic Instruments Corporation, Mahwah, NJ.

III. EXPERIMENTAL RESULTS

A. *DSC Measurement on the Cold-Rolled Specimens*

Figure 1 shows the DSC curves for the 5 pct cold-rolled $Ti_{50}N_{50}$ specimen in the first heating cycle and subsequent cooling and heating cycles. Compared with the experimental results of the internal friction testing[19] and electrical resistance measurements,[25] the DSC peaks shown in Figure 1 are associated with the martensitic transformation of $B2 \leftrightarrow B19'$ ($B2$: parent phase, CsCl-type structure; $B19'$: martensite, monoclinic distortion of the $B19$ structure). The first heating curve shows an endothermic reaction, with ΔH being 16.55 J/g and the peak temperature A_1^* near 101.9 °C. The cooling curve, however, shows an exothermic reaction, with ΔH being 24.16 J/g and the peak temperature M^* near 37.9 °C. In the second heating curve, A_2^* appears at 75.7 °C, with ΔH = 24.57 J/g.

Figures 2(a) and (b) show the DSC curves of the first heating cycle and subsequent cooling and heating cycles, respectively, for the 20 pct cold-rolled specimen. In Figure 2(a), peak A_1^* appears at 135.4 °C. In Figure 2(b), there are two separate peaks on the cooling run; one is associated with the martensitic transformation, M^* = 16.9 °C, and the other is associated with the R-phase transformation, R_C^* = 47.6 °C (R phase: intermediate phase, rhombohedral structure). However, on the following heating run, only an endothermic peak A_2^* appears at 67.3 °C. If cooling is stopped at 37 °C (between M^* and R_C^* temperatures) and then resumed, another peak R_H^* appears before the A_2^* peak at about 57.4 °C (shown as the dashed line in Figure 2(b)). This implies that the martensite phase is more stable than the R phase before transforming to $B2$ phase during the heating cycle. Figure 2(b) indicates that the transformation sequence of the 20 pct cold-rolled specimen is $B2 \rightarrow R \rightarrow B19'$ on cooling and $B19' \rightarrow B2$ on heating.

Figures 3(a) and (b) show the same curves as Figures 2(a) and (b), this time for the 40 pct cold-rolled specimen. In Figure 3(b), there are also two separate peaks on the cooling run, M^* = 8.0 °C, R_C^* = 52.1 °C. On the heating run, there is a duplex peak contributed by both the martensitic and R-phase transformations. When the measurement on the cooling run is stopped at 37 °C (between M^* and R_C^*) and again resumed, the peak R_H^* appears after the peak A_2^* at about 63.3 °C (shown as the dashed line in Figure 3(b)). This means that $B19' \rightarrow R$ transformation occurs before $R \rightarrow B2$ transformation. The DSC curves for both the as-annealed and 10 pct cold-rolled specimens are similar to those shown in Figure 1, except for the difference of peak temperatures and ΔH values, and, hence, are omitted here. All experimental results, including peak temperatures and ΔH values, are summarized in Table I. The data in Table I are also plotted in Figures 4 and 5 for A_1^* and

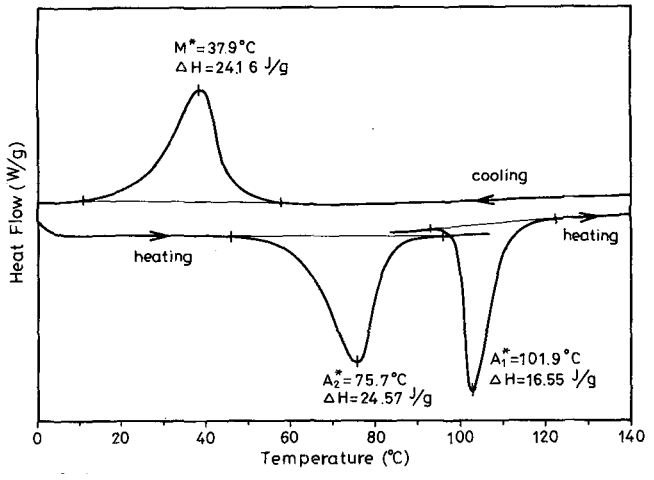

Fig. 1—DSC curves for the as-annealed $Ti_{50}Ni_{50}$ alloy.

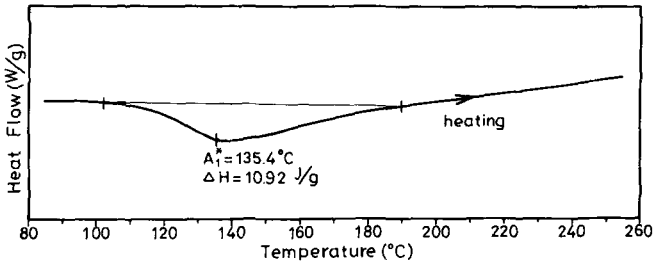

(*a*)

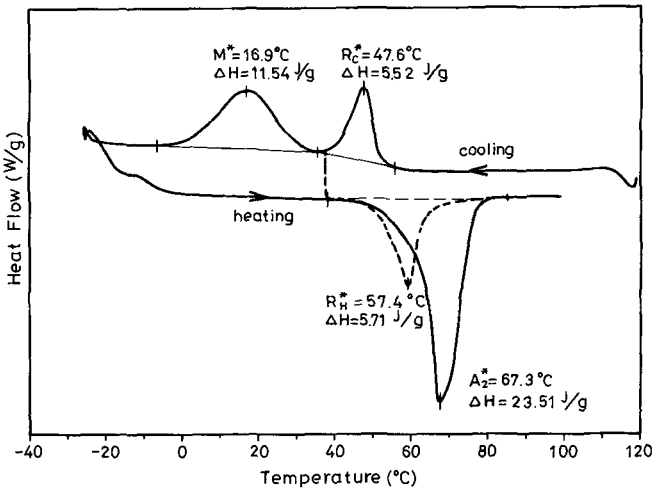

(*b*)

Fig. 2—DSC curves for the 20 pct cold-rolled $Ti_{50}Ni_{50}$ alloy: (*a*) the first heating run and (*b*) the following cooling and heating runs.

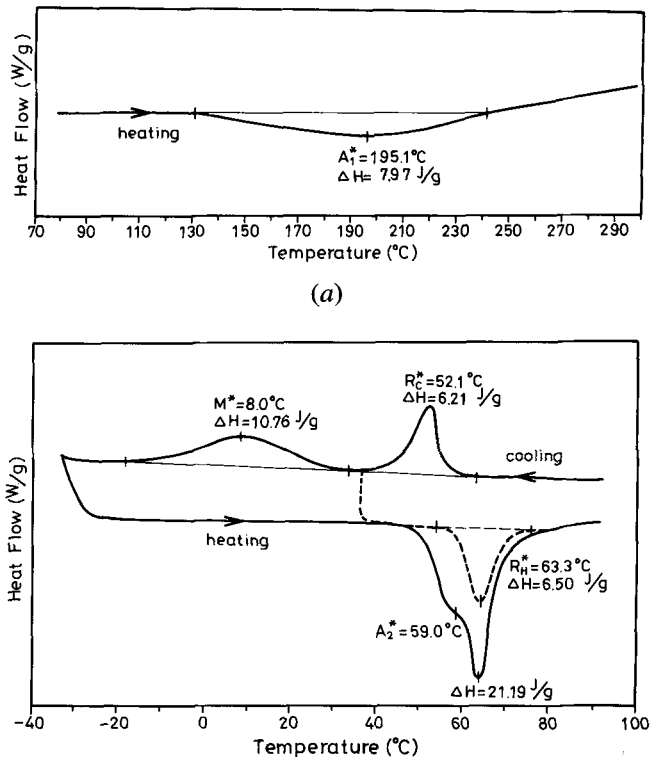

Fig. 3—DSC curves for the 40 pct cold-rolled $Ti_{50}Ni_{50}$ alloy: (*a*) the first heating run and (*b*) the following cooling and heating runs.

$\Delta H(A_1^*)$ *vs* thickness reduction and for M^*, A_2^*, R_C^*, R_H^* *vs* thickness reduction, respectively. The characteristics shown in Figures 4 and 5 will be discussed in Section IV.

B. *XRD Measurement of Cold-Rolled Specimens*

Figures 6(a) through (f) show XRD patterns of cold-rolled equiatomic TiNi alloy with various thickness reductions. The typical XRD spectra for as-annealed TiNi martensite are shown in Figure 6(a). After cold rolling, as shown in Figures 6(b) through (e), the line intensity of martensite spectra decreases; but the parent $B2$ phase appears and reaches the maximum value at 10 pct degree of cold rolling, then recedes and broadens at 20 and 40 pct of cold rolling. If the cold-rolled specimens are subjected to a reverse martensitic transformation, the diffraction peak of the $B2$ phase disappears and the diffraction spectra recover to the martensite spectra, as shown in Figure 6(f), which is similar to Figure 6(a). We will discuss these interesting characteristics in Section IV.

C. *Hardness Test of Cold-Rolled Specimens*

Figure 7 shows the hardness (*Hv*) *vs* thickness reduction for the cold-rolled equiatomic TiNi alloy at room temperature. In Figure 7, curve A is the hardness of the as-cold-rolled specimens; curve B is the hardness of the same specimens subjected to a reverse martensitic transformation of $B19' \rightarrow B2$ and then to a forward martensitic transformation of $B2 \rightarrow B19'$. In Figure 7, both curves A and B increase with increasing degree of thickness reduction, but the hardness of curve B is always lower than that of curve A, especially when the thickness reduction is more than 5 pct. The features appearing in Figure 7 will also be discussed in Section IV.

IV. DISCUSSION

A. *Martensite Stabilization and Stress-Induced Parent Phase (SIP) in the Cold-Rolled Equiatomic TiNi Alloy*

We studied the cold-rolled equiatomic TiNi alloy by TEM observation in our previous article.[19] That study revealed a variety of deformed martensite morphologies. In addition to those deformed morphologies, though, other deformed features are induced during cold rolling, such as dislocations and vacancies. Due to the complex morphologies existing in the deformed martensite, however, dislocations and vacancies are shielded and not easily detected by TEM. As mentioned in the Introduction, these deformed structures seem to be related to the martensite stabilization.[19] Differential scanning calorimetry measurements also indicate the martensite stabilization, as shown in Figure 4, where the reverse martensitic transformation temperature A_1^* shifts to a higher value with increasing degree of cold rolling. After the occurrence of the first reverse martensitic transformation of $B19' \rightarrow B2$, the characteristic of martensite stabilization disappears, as indicated by the M^* and A_2^* temperatures in

Table I. Peak Temperature and ΔH Values of A_1^*, A_2^*, M^*, R_C^*, and R_H^* at Various Degrees of Cold Rolling

Cold Rolling	0 Pct	5 Pct	10 Pct	20 Pct	40 Pct
A_1^* (°C)	86.1	101.9	117.6	135.4	195.1
ΔH (J/g)	25.16	16.55	13.40	10.92	7.97
A_2^* (°C)	86.1	75.7	72.3	67.3	59.0
ΔH (J/g)	25.16	24.57	24.01	23 51	—
M^* (°C)	45.8	37.9	29.7	16.9	8.0
ΔH (J/g)	23.98	24.16	22.73	11.54	10.76
R_C^* (°C)	—	—	37.4*	47.6	52.1
ΔH (J/g)	—	—	—	5.52	6.21
R_H^* (°C)	—	—	—	57.4	63.3
ΔH (J/g)	—	—	—	5.71	6.50

*Duplex peak contributed by both martensitic and R-phase transformations.

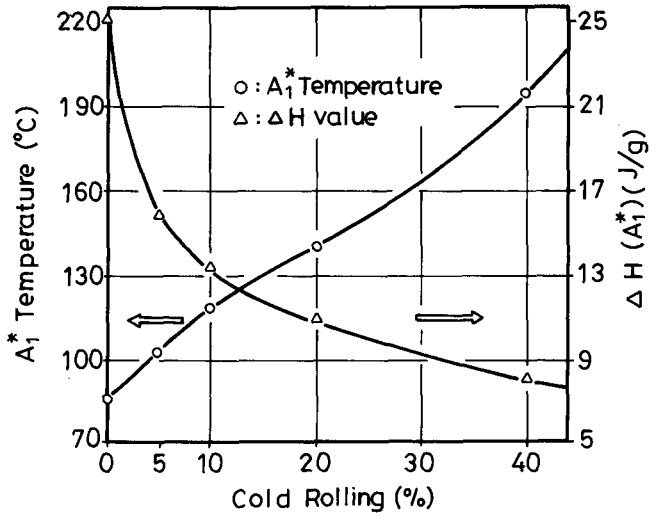

Fig. 4—The A_1^* temperature and $\Delta H(A_1^*)$ value *vs* the degree of cold rolling for the $Ti_{50}Ni_{50}$ alloy.

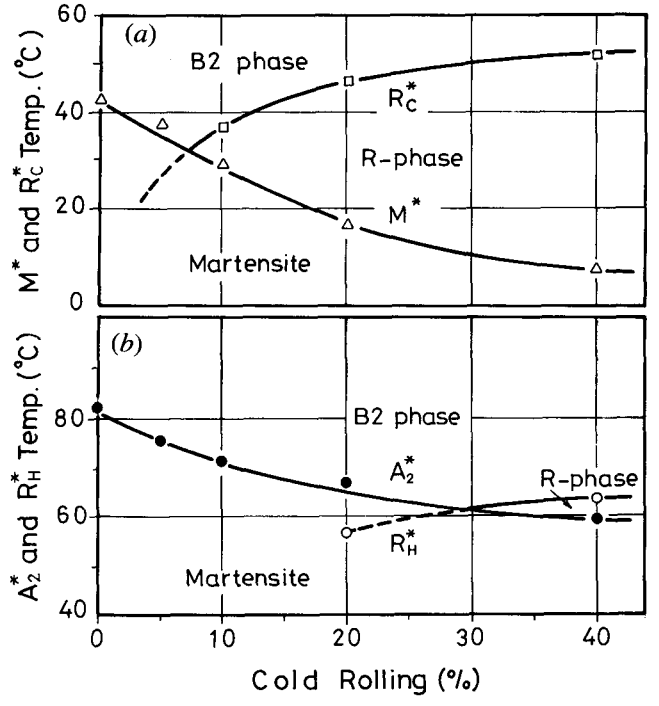

Fig. 5—(*a*) M^* and R_C^* temperatures and (*b*) A_2^* and R_H^* temperatures *vs* the degree of cold-rolling for the $Ti_{50}Ni_{50}$ alloy.

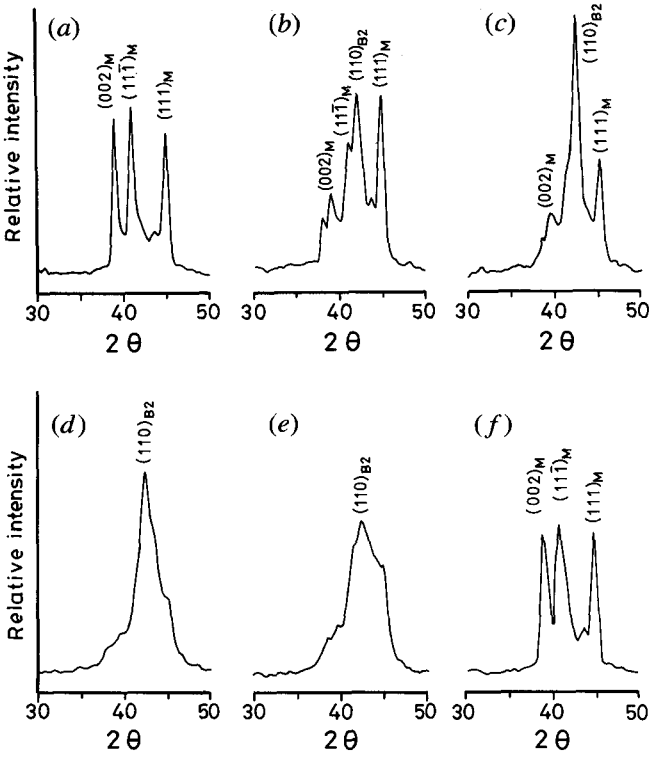

Fig. 6—The XRD spectra for the cold-rolled $Ti_{50}Ni_{50}$ alloy: (*a*) as-annealed, (*b*) 5 pct, (*c*) 10 pct, (*d*) 20 pct, (*e*) 40 pct, and (*f*) specimen (d) subjected to a reverse and forward martensitic transformation.

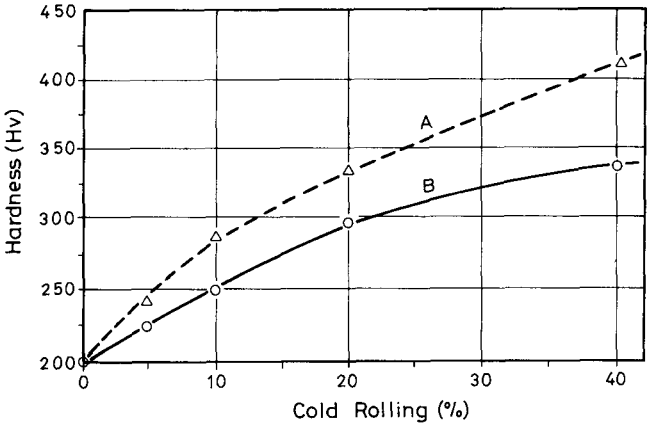

Fig. 7—Microhardness *vs* the degree of cold rolling for the $Ti_{50}Ni_{50}$ alloy. Curves A and B indicate the hardness of the deformed martensite without and with the first reverse martensitic transformation, respectively.

Table I. Although the martensite stabilization disappears, the deformation-induced dislocations remain in the deformed specimens and affect their subsequent transformation behaviors. The M^* and A_2^* temperatures decrease, then, with increasing degree of cold rolling. The hardness test results shown in Figure 7 also support this conclusion: curves B and A show the hardness of the deformed martensite with and without the first reverse martensitic transformation of $B19' \rightarrow B2$, respectively. There are plenty of dislocations retained in the martensite of curve B. The hardness difference between curves A and B comes from the disappearance of deformed structures and the annihilation of vacancies in the martensite.[19] The increasing *Hv* value of curve B with the increasing thickness reduction is suggested to come from the increasing number of deformation-induced dislocations which remain in the martensite after the martensite stabilization vanishes.

In order to reveal more clearly the deformed structures induced by cold rolling, the XRD technique is used, and the results are shown in Figure 6. In Figure 6, the SIP is introduced in the cold-rolled martensite. The appearance of SIP was implicitly reported in Reference 24, in

which the parent $B2$ phase can be induced from the martensite by the tensile deformation in the $Ti_{51}Ni_{49}$ alloy. The reason for the formation of SIP, however, remains obscure in their report. Here, we will discuss the formation of SIP as follows.

Mercier *et al.*[26] and Lotkov *et al.*[27] investigated the anomalies of the elastic properties of TiNi single crystals using the ultrasonic resonance method. They reported that the lattice softening phenomenon exists around the forward martensitic transformation temperature for TiNi alloys and promotes the shear transformation by thermal or mechanical driving forces. Lattice softening has also been predicted to occur in the martensite phase prior to the reverse transformation to $B2$ phase upon heating,[28] for example, in a Cu-Zn-Al martensite single crystal.[29] If this behavior can also occur in the TiNi martensite around the A_s temperature, the martensite could be stress-induced to the parent $B2$ phase. In other words, the lattice softening phenomenon existing around the reverse martensitic transformation temperature for TiNi alloy could promote the formation of SIP. In this study, the cold rolling temperature (about 25 °C) is quite near the A_s temperature (about 60 °C). During cold rolling, the stress distribution in the deformed specimen is quite complex, and some martensite plates now have the chance to be induced to SIP by the rolling stress, although most of the deformation strain is accommodated by the deformed martensite morphologies. After the rolling process, SIP is still retained, because the internal stress existing within the deformed martensite impedes the recovery of SIP to martensite. The higher the degree of cold rolling, the more the martensite plates are induced to SIP. But for the severely deformed specimens, the SIP $B2$ phase is also partially deformed, and the XRD spectra of $B2$ phase are therefore broadened.

B. *Heats of Transformations in the Cold-Rolled Equiatomic TiNi Alloy*

Based on thermodynamic analysis of a thermally induced thermoelastic transformation,[30,31] the transformation heat ΔH measured by the calorimeter is the sum of (1) the chemical enthalpy change, ΔH_{ch}, (2) the stored elastic strain enthalpy change, ΔH_{el}, and (3) the energy consumed in the form of frictional work, E_{fr}. In other words, the transformation heat ΔH can be expressed by Eq. [1]:

$$\Delta H = \Delta H_{ch} - \Delta H_{el} + E_{fr} \qquad [1]$$

In Figure 4, the ΔH value of the first reverse martensitic transformation, $\Delta H(A_1^*)$, decreases quickly with increasing thickness reduction, especially for the ≤ 10 pct thickness-reduced specimens. The ΔH decrement can reach 17 J/g for the 40 pct thickness-reduced specimen. This behavior is unusual for a thermoelastic martensitic transformation, in which the ΔH value should increase with increasing transformation temperature. In fact, the ΔH decrement for cold-rolled shape memory alloys has also been found in $Ti_{51}Ni_{49}$[32] and $Ti_{50}Ni_{20}Pd_{30}$[33] alloys and has been implicitly reported in the Cu-Zn-Al alloy.[34]

1. *Factors affecting the transformation heat in the cold-rolled equiatomic TiNi alloy*

Why does the $\Delta H(A_1^*)$ decrease significantly after cold rolling in the equiatomic TiNi alloy? We suspect that the decrement of ΔH values may be due to the incompletion of the reverse transformation. But examining the following cooling and heating runs, the ΔH are found to recover to the normal values, say 23 to 25 J/g in Table I. Hence, the first reverse transformation of $B19' \rightarrow B2$ is believed to be transformed completely. However, in order to explain the unusual characteristic of ΔH decrement indicated in Figure 4, we propose three possible contributions:

a. *The effect of SIP*

As discussed in Section IV–A, a portion of martensite has been reversely transformed to SIP by mechanical stress during cold rolling. Therefore, a smaller volume of martensite is transformable to $B2$ phase during the heating run. This will reduce the needed endothermic heat because ΔH is averaged by the total material weight. The ΔH value of Figure 4 decreases sharply in the early 10 pct degree of cold rolling. This feature is quite consistent with the XRD results of Figure 6, in which the line intensity of $B2$ phase also increases quickly in the early 10 pct degree of cold rolling.

b. *The effect of accumulated elastic energy*

It is well known that variants of thermoelastic martensite can be reoriented to a preferred direction under the deformation. It is reasonable to suggest that the accumulated elastic energy stored in the accommodated variants is increased by increasing the degree of deformation. During the reverse transformation, this accumulated elastic energy is released to increase the ΔH_{el} and reduces the needed transformation ΔH value. Melton and Mercier[35] pointed out that the stored elastic energy in the stress-induced martensite is more than that in the thermally induced martensite. This characteristic supports the above suggestion, because the stress-induced martensite also orients variants to a preferred direction under the mechanical stress.

c. *The effect of defect recovery*

As mentioned in Section IV–A, a variety of deformed structures can be induced after cold rolling. Most of these deformed defects recover gradually when the cold-rolled specimens are reheated. During this recovery period, the internal energy of deformed specimens gradually decreases, and the recovery heat is gradually released. We suggest that this recovery process can be accelerated by the reverse martensitic transformation because a driving force exists to relieve these deformed structures during the reverse martensitic transformation. As reported in Reference 36, a quantity of stored energy in a deformed metal can be released during the recovery process. Hence, the detectable ΔH value should be lowered during the reverse martensitic transformation.

2. *The effect of cold-rolling extent on the transformation heat*

As mentioned in Section 1, the decrement of $\Delta H(A_1^*)$ seems to be caused by three factors, but it is difficult to determine which factor is the most significant. In general, TiNi alloys have a 7 to 8 pct recoverable shape memory strain. In this deformation range, the deformation strain should be accommodated by the preferred martensite variants and significant work energy stored in the accumulated elastic energy. In addition, SIP also plays a part, as indicated in Figure 6, where the line intensity

of SIP increases to a maximum value at 10 pct degree of cold rolling. Results suggest that effects of SIP and accumulated elastic energy have the major effect in the early 10 pct degree of cold rolling. When the degree of cold rolling is larger than 10 pct, however, a variety of deformed martensite morphologies appear,[19] and the line intensity of SIP broadens (Figure 6). This indicates that the deformation strain is not accommodated by martensite variants or SIP but by some other defect, such as dislocations/vacancies. At this time, the contribution of defect recovery is the major factor in the specimens with more than 10 pct degree of cold rolling.

For the cold-rolled TiNi alloys, the transformation heat ΔH for the first reverse martensitic transformation can be modified from Eq. [1] and expressed as follows:

$$\Delta H = \Delta H_{ch} - \Delta H_{el} + E_{fr} - \Delta H_{cr} \qquad [2]$$

In Eq. [2], ΔH_{cr} is the extra term for the cold-rolled specimens and is contributed by SIP and defect recovery. The ΔH_{el} in Eq. [2] will be increased when accumulated elastic energy by cold rolling is added.

C. *Effects of Cold Rolling on the Phase Transformation of the Equiatomic TiNi Alloy*

As discussed in Section A, the alloy retains a significant number of dislocations after the deformed martensite is subjected to a reverse transformation of $B19' \rightarrow B2$. In other words, during the first reverse martensitic transformation, most of the deformed structures vanish, but many dislocations remain to affect the subsequent transformation behaviors. In Figure 5, peak temperatures M^* and A_2^* decrease with increasing thickness reduction, due to the fact that the martensitic transformation temperatures in TiNi alloy can be depressed by the retained dislocations.[12,18,19,37] The higher the dislocations retained in the cold-rolled specimens, the lower will be their M^* and A_2^* temperatures.

In Figures 2 and 3, it is seen that R-phase transformation can appear on cooling and heating runs if the thickness reduction is larger than 20 and 40 pct, respectively. We suggest that the appearance of the R phase is also related to the retained dislocations after cold rolling. As shown in Figures 5(a) and (b), the retained dislocations depress the M^* and A_2^* temperatures, but they raise the R_C^* temperature slightly. If $M^* < R_C^*$, then R phase appears prior to martensitic transformation during the cooling. If $A_2^* < R_H^*$, then martensite will transform to R phase before it transforms to $B2$ phase. Carefully examining Figure 5(a), when the degree of cold rolling is less than 7 pct (intersection of R_C^* curve and M^* curve), only the $B2 \rightarrow B19'$ transformation appears in the cooling process because $R_C^* < M^*$. When the degree of cold rolling is more than 7 pct, the transformation sequence changes to $B2 \rightarrow R \rightarrow B19'$ because $R_C^* > M^*$. The same situation appears in the heating process. As shown in Figure 5(b), when the degree of cold rolling is less than about 30 pct (intersection of R_H^* curve and A_2^* curve), only $B19' \rightarrow B2$ transformation appears because $R_H^* < A_2^*$. But if the degree of cold rolling is more than 30 pct, the transformation sequence changes to $B19' \rightarrow R \rightarrow B2$, due to $R_H^* > A_2^*$.

In our previous article,[19] the R-phase transformation induced by cold rolling in $Ti_{50}Ni_{50}$ alloy is not obvious in the internal friction and shear modulus measurements. In this study, however, the R-phase transformation stands out in the DSC measurement. This discrepancy may come from the different sensitivities of the R-phase transformation to these measuring techniques. In our work on thermal cycling,[25] the internal friction peak of the R-phase transformation does not appear either, although there is an obvious peak of R-phase transformation in the DSC curves for the same specimen.

V. CONCLUSIONS

The martensitic transformation heat ΔH in a cold-rolled equiatomic TiNi alloy has been studied systematically by DSC measurements, hardness tests, and XRD. The important conclusions are as follows:

1. The martensite stabilization and SIP $B2$ phase are introduced in the cold-rolled martensite. The formation of SIP appears to be related to the lattice softening phenomenon occurring in martensite around the A_s temperature.
2. The ΔH value of the first reverse martensitic transformation decreases enormously and quickly with the increasing degree of cold rolling. Three factors may be responsible for this ΔH decrement: (1) the occurrence of the SIP, which reduces the transformable martensite volume; (2) the release of the accumulated elastic energy, which is induced by the cold rolling and stored in the accommodated martensite variants; and (3) the recovery defects induced by cold rolling and release of the recovery heat.
3. After the first reverse martensitic transformation, the deformation-induced dislocations may remain in the cold-rolled alloy, depress the martensitic transformation temperatures, and hence induce the R-phase transformation.

ACKNOWLEDGMENT

The authors are pleased to acknowledge the financial support of this research by the National Science Council (NSC), Republic of China, under Grant Nos. NSC 78-0405-E002-18 and NSC 80-0405-E002-23.

REFERENCES

1. S. Miyazaki, K. Otsuka, and Y. Suzuki: *Scripta Metall.*, 1981, vol. 15, pp. 287-92.
2. G.D. Sandrock, A.J. Perkins, and R.F. Hehemann: *Metall. Trans.*, 1971, vol. 2, pp. 2769-81.
3. K. Otsuka, T. Sawamura, and K. Shimizu: *Phys. Status Solidi A*, 1971, vol. 5, pp. 457-70.
4. H.C. Ling and R. Kaplow: *Metall. Trans. A*, 1981, vol. 12A, pp. 2101-11.
5. S. Miyazaki, Y. Ohmi, K. Otsuka, and Y. Suzuki: *ICOMAT-82, J. Phys.*, 1982, vol. 43, pp. C4-255-60.
6. S. Miyazaki, T. Imai, Y. Igo, and K. Otsuka: *Metall. Trans. A*, 1986, vol. 17A, pp. 115-20.
7. C.M. Hwang, M. Meichle, M.B. Salamon, and C.M. Wayman: *Phil. Mag.*, 1983, vol. 47A, pp. 9-30, 31-62, and 177-91.
8. S.K. Wu and C.M. Wayman: *Mater. Sci. Eng.*, 1987, vol. 96, pp. 295-302.
9. M. Nishida, C.M. Waymann, and T. Honma: *Metallography*, 1986, vol. 19, pp. 99-113.

10. C.M. Hwang and C.M. Wayman: *Scripta Metall.*, 1983, vol. 17, pp. 1449-53.
11. T. Tadaki, Y. Nakata, and K. Shimizu: *Trans. Jpn. Inst. Met.*, 1987, vol. 28, pp. 883-90.
12. S. Miyazaki, Y. Igo, and K. Otsuka: *Acta Metall.*, 1986, vol. 34, pp. 2045-51.
13. S.K. Wu, H.C. Lin, and T.S. Chou: *Acta Metall.*, 1990, vol. 38, pp. 95-102.
14. M. Nishida and T. Honma: *Scripta Metall.*, 1984, vol. 18, pp. 1293-98.
15. M. Nishida and C.M. Wayman: *Scripta Metall.*, 1984, vol. 18, pp. 1389-94.
16. S.K. Wu and H.C. Lin: *Scripta Metall. Mater.*, 1991, vol. 25, pp. 1295-98.
17. Y. Okamoto, H. Hamanaka, F. Miura, H. Tamura, and H. Horikawa: *Scripta Metall.*, 1988, vol. 22, pp. 517-20.
18. T. Todoroki and H. Tamura: *Trans. Jpn. Inst. Met.*, 1987, vol. 28, pp. 83-94.
19. H.C. Lin, S.K. Wu, T.S. Chou, and H.P. Kao: *Acta Metall. Mater.*, 1991, vol. 39, pp. 2069-80.
20. S. Miyazaki and K. Otsuka: *Metall. Trans. A*, 1986, vol. 17A, pp. 53-63.
21. D.M. Coldstein, L. Kabacoff, and J. Tydings: *J. Met.*, 1987, March, pp. 19-26.
22. O. Mercier and E. Torok: *ICOMAT-82, J. Phys.*, 1982, vol. 43, pp. C4-267-72.
23. D.M. Goldstein: Naval Surface Weapons Center, Dahlgren, VA, TR87-126, 1987, p. 126.
24. Y.K. Kovneristy, S.G. Fedotov, and L.A. Matlakhova: *Proc. Int. Shape Memory Alloy Symp.*, Guilin, China, 1986, pp. 175-180.
25. H.C. Lin and S.K. Wu: National Taiwan University, Taipei, Taiwan, unpublished research, 1992.
26. O. Mercier, K.N. Melton, G. Gremaud, and J. Hagi: *J. Appl. Phys.*, 1980, vol. 41, pp. 1833-34.
27. A.I. Lotkov, A.V. Kuznetsov, V.N. Griskov, and A.A. Botaki: *Proc. Int. Shape Memory Alloy Symp.*, Guilin, China, 1986, pp. 153-58.
28. N. Nakanishi: in *Shape Memory Effect in Alloys*, J. Perkins, ed., Plenum Press, New York, NY, 1975, pp. 147-75.
29. G. Guenin and P.F. Gobin: *ICOMAT-79*, 1979, pp. 316-321.
30. H.C. Tong and C.M. Wayman: *Acta Metall.*, 1975, vol. 23, pp. 209-15.
31. J. Ortin and A. Planes: *Acta Metall.*, 1988, vol. 36, pp. 1873-89.
32. H.C. Lin, S.K. Wu, and J.C. Lin: *ICOMAT-92*, 1992, in press.
33. Y.C. Lo, S.K. Wu, and H.C. Lin: National Taiwan University, Taipei, Taiwan, unpublished research, 1992.
34. K. Adachi and J. Perkins: *Metall. Trans. A*, 1986, vol. 17A, pp. 945-59.
35. K.N. Melton and O. Mercier: *Acta Metall.*, 1981, vol. 29, pp. 393-98.
36. R.W. Cahn and P. Haasen: *Physical Metallurgy*, 3rd ed., Elsevier Science Publishers B.V., Amsterdam, The Netherlands, 1983, ch. 25.
37. D.N. Abujudom, P.E. Thoma, and S. Fariabi: *ICOMAT-89*, 1989, pp. 565-70.